JOURNAL OF MATERIALS SCIENCE 23 (1988) 2133–2141

Phase relations and hydrogen absorption of neodymium–iron–(boron) alloys

BERNHARD RUPP*, ALEX RESNIK, DAVID SHALTIEL
Racah Institute of Physics, The Hebrew University, IL 91904 Jerusalem, Israel

PETER ROGL
Institut für Physikalische Chemie, der Universität Wien, Währingerstrasse 42, A 1090 Vienna, Austria

Based on an investigation of the phase correlations in the system Nd–Fe–B, a complete study of the hydrogen absorption of Nd–Fe–B alloys is presented, mainly concerning the permanent magnet material $Nd_2Fe_{14}B$. Absorption isotherms of the compound $Nd_2Fe_{14}B$ and of the master alloy for permanent magnet production, $Nd_{15}Fe_{77}B_8$, have been recorded and their hydrogenation behaviour is discussed. Thermal desorption spectra support the conclusion that neodymium hydride is the second hydride phase in the hydrogenated master alloy. In the Nd–Fe binary system, Nd_2Fe_{17} was confirmed as the only equilibrium phase at 870 and 1170 K. The properties of a new ferromagnetic ternary hydride $Nd_2Fe_{17}H_x$, $x = 0$ to 5, with the Th_2Zn_{17} type structure, space group $R\bar{3}m$, are reported.

1. Introduction

A new family of commercial cobalt- and samarium-free rare earth permanent magnets is essentially based on alloys of the nominal composition $Nd_{15}Fe_{77}B_8$ ("Neomax"): the tetragonal compound $Nd_2Fe_{14}B$, with its high magneto-crystalline anisotropy, is the main constituent of the sintered high-coercivity permanent magnets. The required small particles of this compound being aligned in a magnetic field before sintering may be produced by (a) mechanical grinding or milling the as-cast material under protective atmospheres (see e.g. Sagawa *et al.* [1, 2]), by (b) rapid solidification (melt-spun alloys, Croat *et al.* [3]), by (c) a new liquid dynamic compaction method (Tanigawa *et al.* [4]) or by (d) a ternary diffusion reaction (Stadelmaier *et al.* [5]). A less conventional way to achieve this goal by means of powder decrepitation due to hydrogen absorption was recently employed by Harris and co-workers [6, 7], McGuiness *et al.* [8] and Oesterreicher and Abache [9]. A special advantage of the latter method is the absence of the fine debris usually introduced by mechanical grinding.

For a basic understanding of the decrepitation process, a detailed investigation of the hydrogen sorption characteristics of $Nd_2Fe_{14}B$ as well as of its neighbouring Nd–Fe–B phases is of interest. As powder decrepitation usually applies to as-cast material, one has to deal with the equilibrium phases as well as with primary crystallization products and possible metastable phases. A part of this work is thus necessarily concerned with the phase relations with respect to the minor phases in the basic alloy for sintered permanent magnets, $Nd_{15}Fe_{77}B_8$.

1.1. Survey of literature data on phase correlations and on structure

Fig. 1 represents the updated phase diagram based on the ternary equilibria established at 873 K by Chaban *et al.* [10] (see also Rogl [11]) and reinvestigated by Buschow *et al.* [12] including furthermore the two versions of the liquidus projections as reported by Matsuura *et al.* [13] and by Schneider *et al.* [14]. The early liquidus projection by Stadelmaier *et al.* [15] is basically similar; differences between those reported [13–15] were discussed in detail by Schneider *et al.* [14] (see also the review by Buschow [16]). The phase equilibria at 1170 K and below [10, 14, 12] are in qualitative agreement with a partial isothermal section at 923 K reported by Sagawa *et al.* [2] who suggested "$Nd_2Fe_7B_6$" to be the correct composition for the boron-rich ternary compound whose formula $Nd_{1+x}Fe_4B_4$ ($x \sim 0.1$) is now widely accepted from both microprobe and X-ray analysis (see Table I and references cited therein).

As far as the Nd-Fe binary system is concerned, both the compounds, Nd_6Fe_{23} earlier mentioned by Oesterreicher and Oesterreicher [17] and $NdFe_2$ [10], were not confirmed as equilibrium phases. It was, however, shown by Cannon *et al.* [18] and later by Meyer *et al.* [19] that $NdFe_2$ ($MgCu_2$ type, space group Fd3m, $a = 0.745$ nm) is readily obtained under high pressure–high temperature conditions (80 kbar, 1473 K).

According to Fig. 1, the only phases at $T < 1170$ K that can enter the thermodynamic equilibrium with $Nd_2Fe_{14}B$ (T_1) are free neodymium, free iron, binary Nd_2Fe_{17} as well as $Nd_{1+x}Fe_4B_4$ (further referred to as

* *Permanent address and address for correspondence*: Institut für Physikalische Chemie der Universität Wien, Währingerstrasse 42, A 1090 Vienna, Austria.

0022–2461/88 $03.00 + .12

TABLE I Crystallographic data for the binary neodymium–iron phases as well as for the ternary neodymium–iron–borides

Compound	Structure type	Space group	Unit cell dimensions (nm)			c/a	Notes	Refs.
			a	c	V (nm^3)			
Binary compounds: neodymium–iron								
$NdFe_2$	$MgCu_2$	Fd3m	0.7452 (5)		0.41383		DS, 20–28 kbar, 1270 K	[18]
"$NdFe_5$"	$CaCu_5$	P6/mmm	0.4946	0.4170	0.08834	0.843	GU, MS, RS	[35]
$NdFe_7$	Th_2Zn_{17}	R$\bar{3}$m	0.8570	1.2439	0.7912	1.451	PD	[46]
	$Th_2Zn_{17}/CaCu_5$	R$\bar{3}$m	0.8578 (3)	1.2462 (7)	0.7941	1.453	DS, WB, A, see ref. cited	[47]
Nd_2Fe_{17}	Th_2Zn_{17}	R$\bar{3}$m	0.8574	1.2464	0.7935	1.453	DS, MB, see ref. cited	[48]
		R$\bar{3}$m	0.8567 (5)	1.2443 (5)	0.7909	1.452 (1)	ND, A, M	[34]
		R$\bar{3}$m	0.8569 (1)	1.2453 (8)	0.7919 (5)	1.453 (1)	PD Fe-rich	*
Ternary compounds: neodymium–iron–boron								
Nd_2FeB_3	$Pr_{5-x}Co_{2+x}B_6$	R$\bar{3}$m	0.5463 (1)	2.4281 (1)	0.6276	4.445	PD, M, PH, MB	[12]
			0.5469 (1)	2.402 (2)	0.6222	4.392	DS, PH, "$Nd_{5-x}Fe_{2+x}B_6$"	[60]
$Nd_{1+\varepsilon}Fe_4B_4$		$P4_2/n$?	0.7141 (3)	14.457	–	–	SX, M, superstruct. c_{Fe}/c_{Nd} = 41/37	[49]
		Pccn	0.7117	3.507	–	–	SX c_{Fe}/c_{Nd} = 10/9	[50, 51]
	$Sm_{1+\varepsilon}Fe_4B_4$	$P4_2/n$	0.71226 (1)	6.624 (5)	–	–	SX, c_{Fe}/c_{Nd} = 19/17	[52]
'$Nd_2Fe_7B_6$'		tetrag.	0.716	0.391 × 8	1.604	4.369	PD, SX, ED	[2]
$NdFe_4B_4$		P4/ncc	0.709	2.756	1.385	3.887	PD, PH	[9]
		tetrag.	0.709	2.742	1.378	3.867	PD, PH	[15]
$Nd_2Fe_{23}B_3$	$Nd_2Fe_{23}B_3$	I$\bar{4}$3d	1.419	–	2.8572	–	PD, MB, MS ?, RS	[53]
$NdFe_{12}B_6$	$SrNi_{12}B_6$	R$\bar{3}$m	0.9605	0.7549	0.6031	0.7859	PD, M, MS, RS	[20]
$Nd_2Fe_{14}B$†	$Nd_2Fe_{14}B$	$P4_2/mnm$	0.8792	1.2174	0.9410	1.385	PD, M, A	[17, 55, 56]
			0.8804 (5)	1.2205 (5)	0.9460	1.386	SX, A	[57]
			0.8792	1.2190	0.9423	1.386	SX, A	[37]
			0.8797	1.2226	0.9461	1.389	PD, M	[66]
			0.8800	1.2186	0.9437	1.385	PD, M	[58]
			0.880	1.219	0.9440	1.385	ND, A	[62]
			0.8803 (1)	1.2196 (1)	0.9451	1.385	ND, A, M, 293 K	[59]
			0.8783 (1)	1.2209 (2)	0.9418	1.390	ND, A, M, 673 K	[59]
			0.8802 (1)	1.2179 (1)	0.9436	1.384	ND, A, M, 77 K	[59]
			0.8805	1.2204	0.9462	1.386	PD ?, M	[24]
			0.882	1.224	0.9522	1.388	PD, SX, A	[2, 64]
			0.8804	1.2199(10)	0.9455	1.386	PD	[12]
			0.8792	1.2177	0.9413	1.385	PD, M	[65]
			0.880	1.218	0.9432	1.384	PD, PH	[14]
			0.8807	1.2203	0.9465	1.386	PD, M	[26, 63]
			0.8795 (3)	1.2188 (6)	0.9428	1.386	PD	[61]
			0.8799 (3)	1.2209 (8)	0.9453 (9)	1.388	PD	*
			0.8805 (2)	1.2202 (7)	0.9462 (7)	1.386	PD, T_1 in "$Nd_{15}Fe_{77}B_8$"	*
$Nd_2Fe_{17}B$			–	–	–	–	DTA, MS, T > 1400 K	[14]
$Nd_3Fe_{20}B_2$		tetrag.	0.8792	1.2174	0.9410	1.385	PD, M	[54]
$Nd_2Fe_{12}B$		tetrag.	0.880	1.221	0.9455	1.388	PD, M	[13]

Notes:
DS Debye Scherrer.
GU Guinier.
PD Powder diffractometer.
WB Weissenberg.
SX Single crystal.
ND Neutron diffraction.
A Atomic parameters given.
PH Phase diagram.
M Magnetization measurements.
MB Mössbauer spectroscopy.
ED Electron diffraction.
RS Rapid solidification.
MS Metastable phase.
* This work.
† Earlier reported as "$Fe_{16}Nd_3B$" or "$Fe_{21}Nd_3B$".

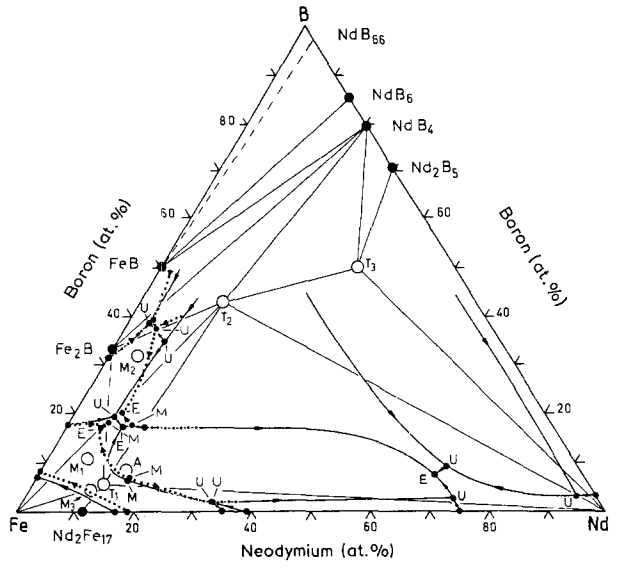

Figure 1 Ternary phase equilibria Nd–Fe–B at 1170 K (670 K for the neodymium-rich part) including liquidus projections from (——) [13] and (· · · ·) [14]. The alternative dashed tieline from T_1 to Fe_2B applies for $T > 1273$ K after [14]. A, nominal composition $Nd_{15}Fe_{77}B_8$ as used for technical permanent magnet material; T_1, $Nd_2Fe_{14}B$; T_2, $Nd_{1.1}Fe_4B_4$; T_3, Nd_2FeB_3; M_1, $Nd_2Fe_{23}B_3$; M_2, $NdFe_{12}B_6$; M_3, $Nd_2Fe_{17}B$; M, melting maximum, E, ternary eutectic point; U, ternary invariancy.

T_2). With respect to the liquidus projection derived [14], pure stoichiometric T_1 forms incongruently from the melt, the primary crystallization product being (Fe), whereas solidification of a melt with the technical alloy composition $Nd_{15}Fe_{77}B_8$ results in primary T_1 followed by secondary $T_1 + T_2$. In this case a part of the intergranular material will form from a neodymium-rich eutectic.

For a correct understanding and interpretation of the hydrogen sorption properties, the exact knowledge of the solidification behaviour, i.e. the final constitution of the solid alloy, is crucial. Besides the equilibrium situation described above, non equilibrium phases may enter the solidification process; these phases may be "true" metastable phases (consisting only of the alloy constituents), and/or phases formed in the technically unavoidable presence of small amounts of oxygen. The new metastable ternary compounds $Nd_2Fe_{23}B_3$ (space group $I\bar{4}3d$) and $NdFe_{12}B_6$ (space group $R\bar{3}m$, $SrNi_{12}B_6$-type) reported recently by Buschow *et al.* [20] to crystallize from amorphous alloys, the metastable alloy $Nd_2Fe_{17}B$ obtained by superheating by Schneider *et al.* [14]; the b c c iron-rich nanometre-size particle phase reported by Hiraga *et al.* [21] and by Sagawa *et al.* [22], and the intergranular b c c neodymium-rich phase observed by Stadelmaier *et al.* [15] (explained as iron containing metastable β-neodymium) are members of the first group. According to Sagawa *et al.* [1, 2] an f c c metallic phase ($a = 0.52$ nm) was claimed to exist containing more than 80 at. % Nd [1] or more than 95 at. % Nd [2]. A summary of the quarternary nanometre-size particle phases detectable only by transmission electron microscopy (TEM) in conjunction with selected-area diffraction (SAD) has been recently given by ElMasry and Stadelmeier [23]. Their explanation for the b c c phase is different to that from other references [21, 22].

Neodymium-rich phases, as well as the oxides or borates mentioned by ElMasry and Stadelmeier [23] were furthermore suggested to play an important role as a liquid-phase sintering aid (see [2, 15]), but the metallic phases only might also be responsible for the easy activation of the permanent magnet material towards hydrogen as mentioned by Harris *et al.* [6].

A comprehensive listing of the crystallographic data concerning stable and metastable phases observed in the Nd–Fe–B ternary system is found from Table I.

1.2. Survey of literature data on hydride formation

The successful application of powder decrepitation [6, 7, 9, 10] has already been emphasized. Hydrides of the pure material $Nd_2Fe_{14}B$ were reported first by Oesterreicher and co-workers [9, 17] and by l'Heritier *et al.* [24], by Dalmas de Reotier *et al.* [25] and by Pourarian *et al.* [26]. Hydrogen absorption and desorption of multiphase technical alloys was studied by Cadogan and Coey [27] by means of thermomanometric analysis combined with Mössbauer spectroscopy. Values for the hydrogen uptake given by these authors differ considerably. The influence of hydrogenation on the magnetic properties of alloys $Nd_{15}Fe_{77}B_8$ was studied by Wiesinger *et al.* [28, 29] using Mössbauer spectroscopy. Neutron diffraction data on $Nd_2Fe_{14}BH_x$ have been announced by Fruchart *et al.* [30] but preprints were not available until now. No data on a hydride of Nd_2Fe_{17} could be found in the current literature (see also the recent review by Buschow [31]).

2. Experimental details

Spherical alloy buttons of 10 to 20 g were obtained by arc melting neodymium (ingot, 99.9%, Rare Earth Products Ltd, UK), iron (rods, 99.96%, Leico Industries, Inc., USA) and boron (crystalline powder, 99.8%, Alpha Ventron, FRG, filled into iron crucibles) with a non-consumable 2% thoriated tungsten electrode on a water-cooled copper hearth under zirconium-gettered high-purity argon. To compensate for boron losses due to the sublimation of boron oxides, an excess of a few milligrams of boron was added beforehand.

Pieces of the ingots were wrapped in molybdenum foil and sealed in argon-filled quartz tubes. After a slow increase of temperature the samples were annealed at 1170 K for 1 week or at 870 K for 3 weeks and then rapidly quenched in water. Qualitative X-ray inspection was made on a Philips powder diffractometer using Cu$K\alpha$ radiation in conjunction with a focusing graphite monochromator. Cell constants were determined by the Guinier technique (monochromatized Cu$K\alpha_1$ radiation) or using double radius Debye–Scherrer cameras (Co$K\alpha$ radiation). In both cases, germanium of > 99.9999% purity ($a_0 = 0.565\,7906$ nm) was added as an internal standard. For the refinement of the cell constants, a least squares fit was employed [32]; powder diffraction intensities were calculated using the LAZY PULVERIX program [33].

Metallographic inspection of the material was done by optical micrography as well as on a Jeol JSM 35

TABLE II Phase analysis of Nd–Fe binary alloys

Composition	Temp. (K)	Phases detected by X-ray diffraction
$NdFe_2$	as-cast	Nd_2Fe_{17} + free (Nd)
	1170	melted, Nd_2Fe_{17} + free (Nd)
	870	as above, + unidentified lines
Nd_6Fe_{23}	as-cast	Nd_2Fe_{17} + free (Nd)
	1170	slightly melted, Nd_2Fe_{17} + free (Nd)
	870	Nd_2Fe_{17}, free (Nd) + unidentified lines
Nd_2Fe_{17}	as-cast	Nd_2Fe_{17} + free (Fe) + free (Nd)
	1170	Nd_2Fe_{17}*
	870	as above

*Small amounts of free iron detected by magnetization measurements.

energy dispersive X-ray analytical system using the LINK 860 software for spectrum analysis.

Absorption isotherms were recorded by adding constant amounts of high-purity hydrogen (99.999%, Matheson Gas Products) into a known volume containing the powdered samples which had been preactivated by a few absorption/degasing cycles. Hydrogen pressures were read from a thermocouple gauge (10^{-3} to 1 mbar), a diaphragm gauge (0.1 to 50 mbar) and a Bourdon type gauge (10 to 1000 mbar). The instruments were calibrated to each other and corrections for dead volumes were applied. Using palladium as a test substance, we obtained excellent pressure–composition isotherms exhibiting horizontal absorption plateaus. The amount of hydrogen uptake of our samples was additionally confirmed by chemical microanalysis in a Perkin Elmer 240 elementary analyser.

Thermal desorption spectra (TDS) of hydrogen were recorded using a quadrupole mass spectrometer while heating hydrogenated samples at a constant rate of $5\,K\,min^{-1}$ in a dynamically pumped liquid-nitrogen-trapped high-vacuum chamber (base pressure better than 10^{-7} mbar).

3. Results and discussion

3.1. Alloy preparation and phase equilibria

3.1.1. Nd–Fe binary alloys

Results of metallographic and X-ray inspection for alloys of the nominal compositions $NdFe_2$, Nd_6Fe_{23} and Nd_2Fe_{17} are summarized in Table II. In agreement with the majority of literature data, peritectically formed Nd_2Fe_{17} is clearly confirmed to be the only binary equilibrium phase in the system Nd–Fe above 870 K under normal pressure conditions. Nd_2Fe_{17} was obtained in single-phase condition after heat treatment at 1170 K for 1 week. Crystallographic data (Table I) are in good agreement with those reported by Herbst *et al.* [34]. Indications for a hexagonal high-temperature modification in rapidly cooled samples were reported by Schneider *et al.* [14]. A full listing concerning homogeneity and cell parameters is presented in Table I including the data for a metastable $CaCu_5$-type phase [35].

There are some indications for a low-temperature phase or an oxygen-stabilized phase [14] at the approximate composition "$NdFe_2$"; however, from the rather weak and blurred X-ray data no detailed analysis was possible. Attempts to stabilize "$NdFe_2$" by small amounts of silicon as known, for example, from $Sc(Sc, Fe, Si)_2$ [36], proved to be unsuccessful.

3.1.2. Nd–Fe–B ternary alloys

In accordance with the phase diagram in Fig. 1, a well-defined single-phase $Nd_2Fe_{14}B$ material can only be obtained after annealing below about 1370 K [20]. The X-ray diffraction pattern of samples quenched from 1170 K were completely indexed in excellent agreement with intensity calculations based on the atom parameters reported by Givord *et al.* [37] (see Fig. 2a). Metallographic inspection showed a minor amount of grain-boundary phases. Despite there being some scatter in the unit cell dimensions reported by different authors (Table I, Fig. 6), there is little doubt about the absence of a homogeneity region (see especially [12]). Whereas small amounts of primary iron were revealed in the as-cast samples, T_2 was found in the as-cast material for technical production, $Nd_{15}Fe_{77}B_8$. The investigation of as-cast and annealed samples with increasing neodymium contents within the three-phase field $Nd–Nd_2Fe_{14}B–Nd_{1.1}Fe_4B_4$ by optical and backscattering electron microscopy revealed a complex microstructure at the grain boundaries (Fig. 3) which can be resolved in detail with high-resolution electron microscopy [22] only. In most cases, however, it was possible to detect areas of free neodymium. In a sample $Nd_{80}Fe_{15}B_5$ with a composition close to the reported neodymium-rich phase we detected only pure neodymium containing virtually no iron in equilibrium with the ternary phases. In agreement with the observations of Stadelmaier *et al.* [15], our X-ray patterns consistently show free neodymium

TABLE III Phase analysis of Nd–Fe–B ternary alloys

Composition	Temp. (K)	Phases detected by X-ray diffraction
$Nd_{80}Fe_{15}B_5$	as-cast	free (Nd), few T_2, T_3?
	870	free (Nd), few T_2
$Nd_{45}Fe_{40}B_{15}$	as-cast	free (Nd), T_1, T_2
	870	as above
$Nd_2Fe_7B_6$	as-cast	T_2, few NdB_4
	1170	as above
$NdFe_4B_4$	as-cast	T_2, Fe_2B, NdB_4
	1170	as above
$Nd_2Fe_{14}B$	as-cast	T_1, few (Fe), T_2?, free (Nd)
	1170	T_1
$Nd_{15}Fe_{77}B_8$	as-cast	T_1, T_2, free (Nd)
	1170	T_1, less T_2, free (Nd)

T_1 indicates $Nd_2Fe_{14}B$.
T_2 indicates $Nd_{1+x}Fe_4B_4$, $x \sim 0.1$.
T_3 indicates Nd_2FeB_3.

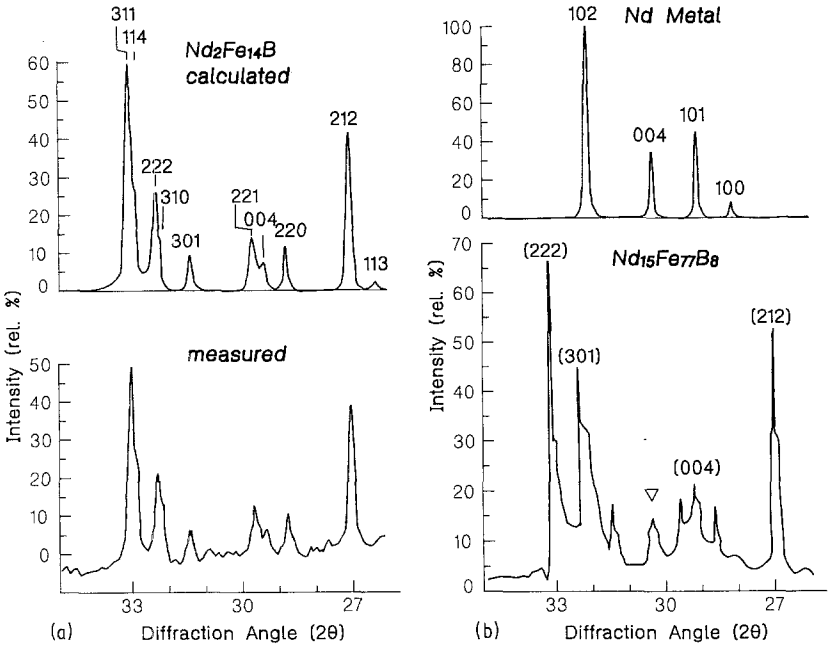

Figure 2 Calculated and measured X-ray diffraction pattern of $Nd_2Fe_{14}B$ (λ = 0.154 178 nm) showing the region sensitive to the presence of alpha neodymium. (b) Comparison between experimental pattern of $Nd_{15}Fe_{77}B_8$ as given in [2] and the pattern of alpha neodymium.

in all samples located in the current three-phase field including $Nd_{15}Fe_{77}B_8$. Results of X-ray diffraction analysis of ternary alloys are summarized in Table III.

In this context we suggest an alternative interpretation of the X-ray diffraction pattern of $Nd_{15}Fe_{77}B_8$ given by Sagawa *et al.* [2]. As seen from the strong intensity misfit in their experimental pattern, the reflection marked by the authors with an empty triangle (claimed to be the (1 1 1) reflection of the "fcc neodymium-rich phase") is not the only excess peak in this area but fits perfectly into the pattern of free α-neodymium (Fig. 2b). We wish to stress that the amount of this "fcc phase" seems to be rather high and that the sharp X-ray deflection contradicts the usually observed small particle size. An alternative interpretation has been suggested by ElMasry and Stadelmaier [23] who address this phase as a "boron-containing fcc NdO".

3.2. Hydrogen absorption

3.2.1. Ternary alloys

To elucidate the hydrogen sorption behaviour of the permanent magnet material, the activation conditions, the equilibrium isotherms and the thermal desorption spectra of pure $Nd_2Fe_{14}B$ were compared with that of as-cast $Nd_{15}Fe_{77}B_8$. The latter is the material ("Neomax") on which the decrepitation technique [6, 7, 9] has been employed.

Activation conditions were established for freshly broken single pieces (about 3 g) of bulk material. For the ternary alloys we did not find a significant difference in the conditions necessary for decrepitation of the bulky pieces, despite the fact that the technical material contained considerable amounts of neodymium in the as-cast as well as in the annealed state. Reaction starts at room temperature after a short incubation time (instantly to a few minutes) from 10 bar on. At 340 K, pressures of about 3 bar led to complete reaction of the materials. It has been reported that crushed powder reacts already at as low a temperature as 370 to 420 K under reduced hydrogen pressure [25]. A significant formation of decomposition products like neodymium or iron a could not be detected in pure material by means of X-ray diffraction under those conditions nor under the long-term treatment during the recording of the isotherms. Application of rigorous conditions such as high pressure (> 30 bar) in combination with high temperature, however, finally led to the formation of free iron and of NdH_2 as proven by X-ray investigation (see also [24, 25, 27, 28]). In all cases the powdered material could be easily ground to suitable particle sizes for a subsequent sintering treatment. It seems that the easy activation of the material is more a result of a self-restoring surface segregation mechanism in analogy to the process found in $LaNi_5$ (see, for example, Schlapbach *et al.* [38]) than an effect promoted by secondary phases.

Pressure–composition isotherms for T_1 and $Nd_{15}Fe_{77}B_8$ are shown in Figs 4 and 5, respectively. The isotherms for both the materials show the same

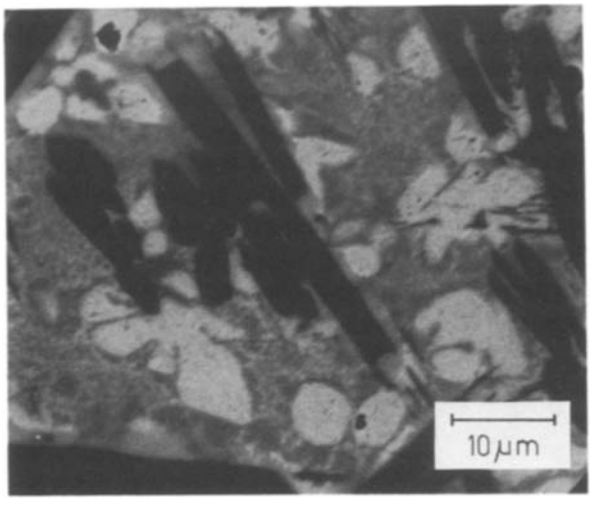

Figure 3 Ternary alloy $Nd_{45}Fe_{40}B_{15}$, backscattering SEM. Black primary crystals: ternary boride T_1; white secondary crystallization product: ternary boride T_2; and eutectic matrix $T_1 + T_2 + (Nd)$. According to the primary constituent the melting trough between T_1 and T_2 near the composition Nd(45)Fe(40)B(15) in Fig. 1 is probably found at slightly lower boron concentrations than reported in [13].

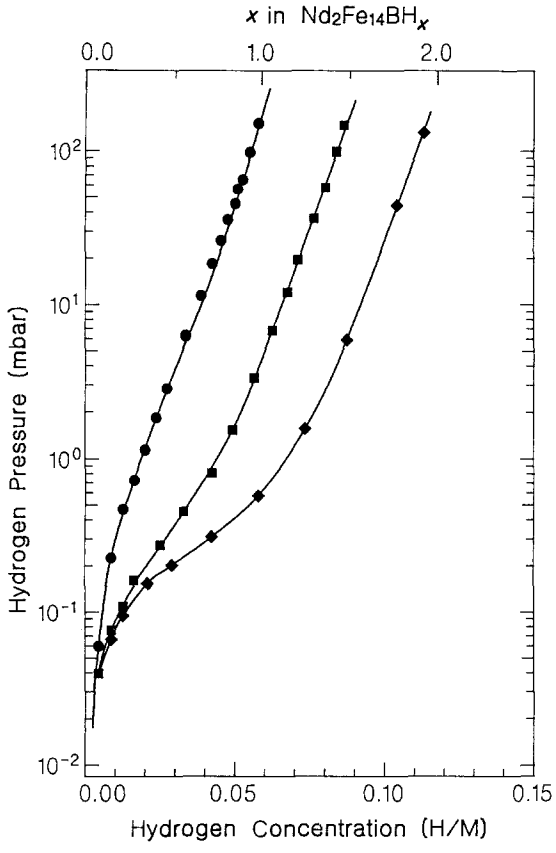

Figure 4 Hydrogen absorption isotherms for pure $Nd_2Fe_{14}B$. H/M = hydrogen to metal ratio counting boron as a metal atom. (●) 570 K, (■) 470 K, (◆) 370 K.

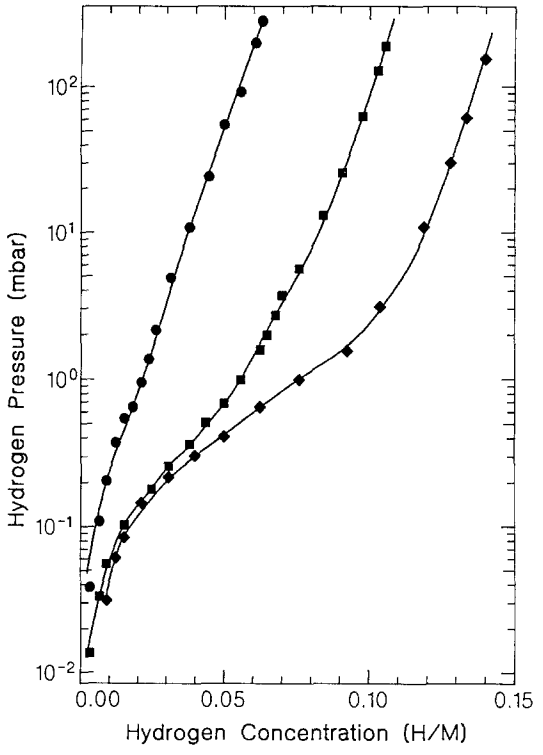

Figure 5 Hydrogen absorption isotherms for as-cast $Nd_{15}Fe_{77}B_8$. H/M = hydrogen to metal ratio counting boron as a metal atom. (●) 570 K, (■) 470 K, (◆) 370 K.

typical shape without absorption plateaus, suggesting the absence of any phase separation due to the formation of distinct stoichiometric phases. The existence of defined stoichiometric phases seems to be excluded from the continuous variation of the lattice parameters with the hydrogen contents (Fig. 6). A similar sigmoid variation of the c parameter has been reported for isotypic compounds $RE_2Fe_{14}BD_x$ by Ferreira *et al.* [39] and Dalmas de Reotier *et al.* [40]. A more pronounced inflection is found for the cerium compound; in the latter case it is probably due to a valence change of the cerium [40]. For the remaining compounds, magnetostrictive effects and/or non-equal size effects for the filling of various tetrahedral voids are to be considered. Approximation of the only slightly bent V against X_H curve by a straight line leads to an average volume increase of 0.0025 nm^3 per hydrogen atom, a value usually found in hydride systems and which compares well with the expansion values obtained for homologous systems [39, 40].

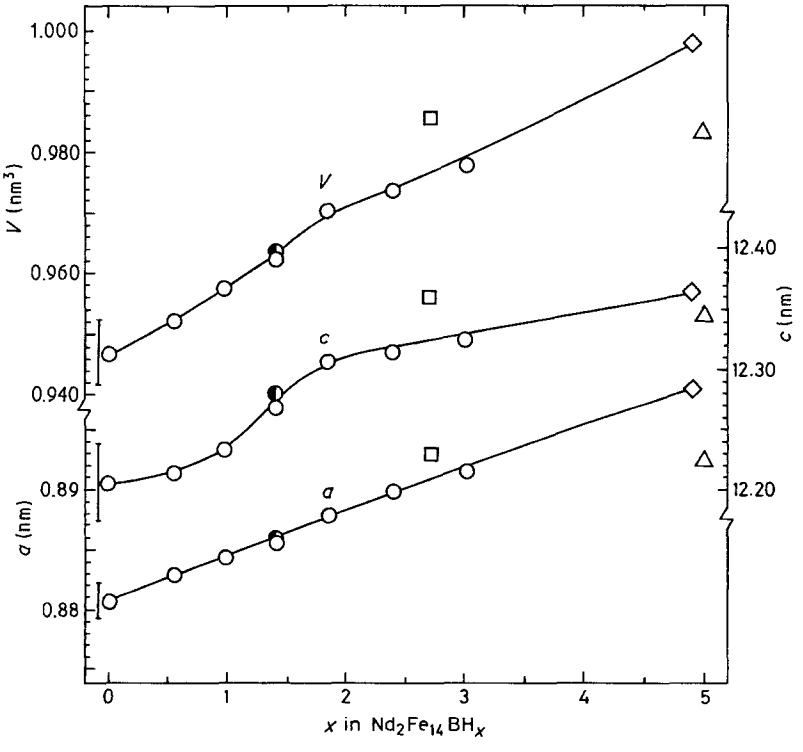

Figure 6 Variation of cell constants with hydrogen content for $Nd_2Fe_{14}B$ including data from (□) [17], (△) [24] and from (◇) [26]. The large error bars cover the range of parameters reported in the literature (Table I) for $X_H = 0$. (○) Guinier, $CuK\alpha_1$, (◐) Debye–Scherrer, $CoK\alpha$.

The amount of hydrogen absorbed in $Nd_2Fe_{14}BH_x$ at room temperature, as estimated for room temperature from Fig. 4 and obtained by chemical analysis (0.28 wt %, $x = 3.0$), is in agreement with the value of 2.7 reported by Oesterreicher and Oesterreicher [17]. Pourarian *et al.* [26] reported enhanced hydrogen uptake ($x = 4.9$) employing an SO_2 sealing technique. A similar high amount of hydrogen uptake was reported by l'Heritier *et al.* [24]; however, their cell parameter data for $Nd_2Fe_{14}BH_5$ are consistently lower than those of Pourarian *et al.* [26] (see Fig. 6) but compare well with the values for $x \sim 3$ which we found to be the maximum load for $Nd_2Fe_{14}B$ if no sealing was used, and charging conditions were as moderate as necessary to avoid decomposition and formation of NdH_2.

The higher amount of hydrogen absorbed by the technical alloy (about $Nd_{15}Fe_{77}B_8H_{26}$, [7]), as compared to the amount absorbed by pure T_1, is probably due to the formation of neodymium hydride as a second hydride phase. Indeed, weak peaks of NdH_2 were present in the X-ray patterns of the hydrided technical material. It should be noted that only 10 at. % of free neodymium in the basic alloy would take up as much hydrogen as the rest of the material. Further proof is obtained from a comparison of the thermal desorption spectra of the magnet material hydrides and of neodymium hydride (Fig. 7): for pure $Nd_2Fe_{14}BH_3$ only one double peak was observed, whereas $Nd_{15}Fe_{77}B_8H_{23}$ spectra show two desorption peaks, the second one at the position of NdH_2. A similar observation of two pressure maxima while degassing the material was reported by Harris and co-workers [6, 7]. The correlation between the relative amounts of hydrogen in the two phases of $Nd_{15}Fe_{77}B_8H_{23}$ (reflected by the areas below the corresponding peaks) and the amount of increase of hydrogen uptake compared to pure material (reflected by the right-hand shift of the corresponding isotherms in Figs 4 and 5) is convincing. The shape of the desorption peak of the pure phase $Nd_2Fe_{14}BH_3$ is similar to those derived for plateauless multisite hydrides (Stern *et al.* [41]): the filling of as much as four different sites (1 RE_3Fe tetrahedron, 8j, and 3 RE_2Fe_2 tetrahedrons, 4e, $16k_1$, $16k_2$) has indeed been reported for the homologous compounds $RE_2Fe_{14}B$

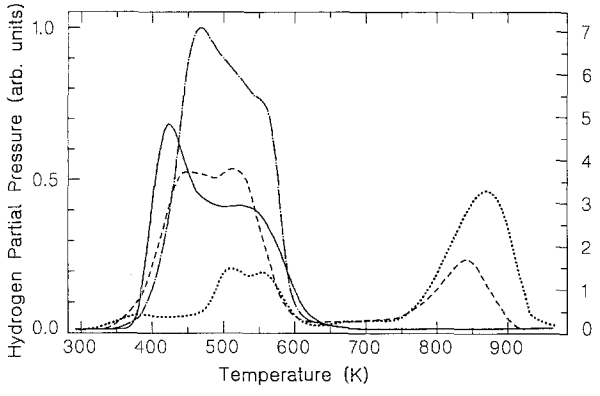

Figure 7 Normalized thermal desorption spectra of hydrides based on the magnetic materials and of powdered neodymium hydride. Heating rate 5 K min^{-1}. Left-hand axis: (——) $Nd_2Fe_{14}B$, (– – –) $Nd_{15}Fe_{77}B_8$, (–·–) Nd_2Fe_{17}. Right-hand axis: (····) Nd.

[39, 40]. A detailed analysis of a series of thermal desorption spectra will be given elsewhere [42]. From X-ray diffraction studies and by simultaneously scanning masses 2 and 18 upon desorption we found that the first peak appearing in the neodymium desorption spectrum is most probably caused by the presence of $Nd(OH)_3$, which forms rapidly on air-exposed surfaces of NdH_2. At 480 K the hydroxide starts to desorb water and to form Nd_2O_3 [43]. The water seems to interact immediately at this temperature with the NdH_2 to yield hydrogen and neodymium oxide. A study under UHV conditions will hopefully help to elucidate this observation [42].

There is another consideration concerning the possibility that the intergranular phase(s) need not necessarily react first – which should lead to a significantly better activation behaviour of the technical alloy compared to pure T_1. As the reaction product of the intergranular phase – regardless of its constitution – is much more stable than T_1 (see TDS) it should, as a result of its high hydrogen content, shift the initial steep part of the absorption isotherm much more to the right-hand side as we observe even in the equilibrium case presented in Fig. 5. It seems that reality (dynamic segregation?) is by far more subtle than a simple superposition of a very stable isotherm (NdH_2) on that of Fig. 4.

To enforce decrepitation of the ternary boron-rich compound T_2, rigorous activation conditions had to be applied (900 to 1000 K, 70 bar). X-ray inspection revealed unaffected bulk material and neodymium hydride as the main decomposition product.

Nd_2FeB_3 (T_3) was not investigated, as it was not expected to play any part in the magnetic alloys.

3.2.2. The binary alloy Nd_2Fe_{17}

Nd_2Fe_{17} reacts readily with hydrogen under cell expansion and forms a ferromagnetic hydride thereby retaining the rhombohedral symmetry of the metal host lattice. It required slightly higher pressures and temperatures to initiate a reaction (30 bar at 370 K), and absorption kinetics were slow compared to the ternary borides. The isotherms, the area below the desorption peak in the normalized thermal desorption spectrum in Fig. 7 and chemical analysis lead to a formula $Nd_2Fe_{17}H_{4.9}$ (0.39 wt % H) for the fully loaded material. A simple comparison between the crystal structures of T_1 and of Nd_2Fe_{17} concerning the stacking sequence of rare earth-containing and iron-containing slabs (RE–Fe–Fe–RE–Fe–Fe–RE for $Nd_2Fe_{14}B$-type structures and RE–Fe–RE–Fe–RE–Fe–RE in the RE_2Fe_{17}-type structure) would, in good qualitative agreement with the experimental findings, predict a maximum filling of 3/2 of that of T_1 ($3 \times 3/2 = 4.5$) in the case of the Nd_2Fe_{17} alloy. As seen from the absorption isotherm in Fig. 8, the Nd–Fe hydride seems to be slightly less stable than the hydride of the ternary boride $Nd_2Fe_{14}B$. No distinct absorption plateaus were observed in agreement with the continuous variation of the unit cell dimensions. The lattice expansion is, however, strongly anisotropic and nonlinear. A detailed study of this puzzling phenomenon, involving neutron diffraction

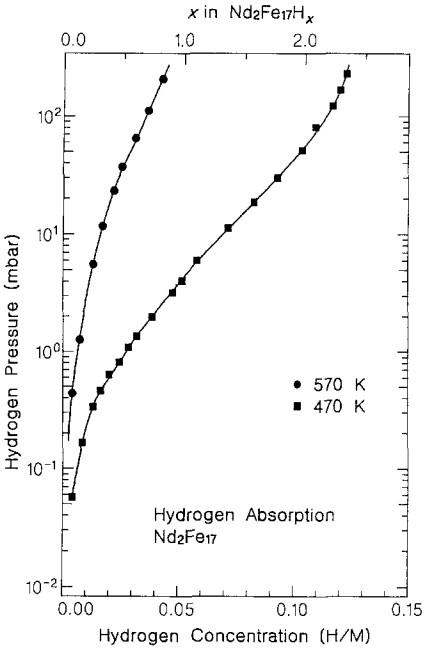

Figure 8 Hydrogen absorption isotherms for Nd_2Fe_{17}. (●) 570 K, (■) 470 K.

[44] and magnetization measurements [45], is in progress.

4. Conclusions

From our investigations we conclude that regardless of the nature of the hydrogen absorbing non-equilibrium neodymium-rich phase, it will decompose into neodymium hydride and most probably iron and, in the case when the neodymium-rich phase is ternary, some boride. This might furthermore account for the observed formation of free iron upon (rigorous) hydrogenation conditions [6, 27]. $Nd_2Fe_{14}B$ may also decompose into iron, T_2 and neodymium, if we follow the equilibrium scenario. However, if iron segregation occurs as a result of a surface process involving oxygen and/or hydrogen, then Nd_2O_3, a hydroxide or a borate could be the decomposition products.

In any case the neodymium-rich metastable phase will not remain in its original state after the hydrogenation. As the magnets sintered from hydrogen decrepitated powder are as good as those produced from milled material [6–8], the effect of the neodymium-rich metastable phases should not be overestimated.

Acknowledgements

This work was partly sponsored under grant no. P5297 of the Austrian Science Foundation (FFWF, Fonds zur Förderung der wissenschaftlichen Forschung in Österreich). The financial support for the Guinier–Huber equipment by the foundation "600 Jahre Wiener Universität" is gratefully acknowledged. B.R. is grateful to the Lady Davis Fellowship Trust and to the Forchheimer Funds for financial support. Thanks are due to M. Reshotko and A. Grayevsky for technical assistance. The help of Avi Ben-Hamo, School of Applied Science and Technology, Hebrew University of Jerusalem, in performing the X-ray microanalysis is kindly acknowledged. We are grateful to J. Zak and S. Frenczko, Microanalytical Laboratory of the Institute of Physical Chemistry, University of Vienna, for the chemical hydrogen analyses.

References

1. M. SAGAWA, S. FUJIMURA, N. TOGAWA, H. YAMAMOTO and Y. MATSUURA, *J. Appl. Phys.* **55** (1984) 2083.
2. M. SAGAWA, S. FUJIMURA, H. YAMAMOTO, Y. MATSUURA and K. HIRAGA, *IEEE Trans. Magn.* **20** (1984) 1584.
3. J. J. CROAT, J. F. HERBST, R. W. LEE and F. E. PINKERTON, *J. Appl. Phys.* **55** (1984) 2078.
4. S. TANIGAWA, Y. HARA, E. J. LAVERNIA, T. S. CHIN, R. C. O'HANDLY and N. J. GRANT, *IEEE Trans. mag.* **22** (1986) 746.
5. H. H. STADELMAIER, N. A. EL MASRY and S. R. STALLRAD, *J. Appl. Phys.* **57** (1985) 4149.
6. I. R. HARRIS, C. NOBLE and T. BAILEY, *J. Less-Common Metals* **106** (1985) L1.
7. I. R. HARRIS, *ibid.* **131** (1987) 245.
8. P. J. McGUINESS, I. R. HARRIS, E. ROZENDAAL, J. OMEROD and M. WARD, *J. Mater. Sci.* **21** (1986) 4107.
9. H. OESTERREICHER and C. ABACHE, *J. Physique* **46** C6 (1985) 49.
10. N. F. CHABAN, YU. B. KUZ'MA, N. S. BILONIZHKO, O. O. KACHMAR and N. V. PETRIV, *Dopov. Akad. Nauk Ukr. RSR. Ser.A* (1980) 875.
11. P. ROGL, in "Handbook on the Physics and Chemistry of Rare Earths", Vol. 6, edited by K. A. Gschneidner, Jr. and L. Eyring (Amsterdam, New York, Oxford, 1984) p. 425.
12. K. H. J. BUSCHOW, D. B. DEMOOIJ, J. L. C. DAAMS and H. M. VAN NOORT, *J. Less-Common Metals* **115** (1986) 375.
13. Y. MATSUURA, S. HISOSAWA, H. YAMAMOTO, S. FUJIMURA, M. SAGAWA and K. OSAMURA, *Jap. J. Appl. Phys.* **24** (1985) L635.
14. G. SCHNEIDER, E. T. HENIG, G. PETZOW and H. H. STADELMAIER, *Z. Metallkde* **77** (1986) 755.
15. H. H. STADELMAIER, N. A. EL MASRY, N. C. LIU and S. F. CHENG, *Mater. Lett.* **2** (1984) 411.
16. K. H. J. BUSCHOW, *Mater. Sci. Rep.* **1** (1986) 1.
17. K. OESTERREICHER and H. OESTERREICHER, *Phys. Status Solidi (a)* **85** (1984) K61.
18. J. F. CANNON, D. L. ROBERTSON and H. T. HALL, *Mater. Res. Bull.* **7** (1972) 5.
19. C. MEYER, F. HARTMANN-BOURTON and Y. GROS, *J. Appl. Phys.* **52** (1981) 2116.
20. K. H. J. BUSCHOW, D. B. DEMOOIJ and H. M. NOORT, *J. Less-Common Metals* **125** (1986) 146.
21. K. HIRAGA, M. HIRABAYASHI, M. SAGAWA and Y. MATSUURA, *Jap. J. Appl. Phys.* **24** (1985) L30.
22. M. SAGAWA, S. HIROSAWA, H. YAMAMOTO, Y. MATSUURA, S. FUJIMURA, H. TOKUHARA and K. HIRAGA, *IEEE Trans. Mag.* **22** (1986) 910.
23. N. A. El MASRY and H. H. STADELMAIER, *Mater. Lett.* **3** (1985) 405.
24. P. l'HERITIER, P. CHAUDOUET, R. MADAR, A. ROUAULT, J. P. SENATEUR and R. FRUCHART, *C.R. Seances Acad. Sci. Ser. 2* **13** (1984) 849.
25. P. DALMAS DE REOTIER, D. FRUCHART, P. WOLFERS, P. VULLIET, A. YAOUANAC, R. FRUCHART and Ph. L'HERITIER, *J. Physique* **46** C6 (1985) 249.
26. F. POURARIAN, M. Q. HUANG and W. E. WALLACE, *J. Less-Common Metals* **120** (1986) 63.
27. J. M. CADOGAN and J. M. D. COEY, *Appl. Phys. Lett.* **48** (1986) 442.
28. G. WIESINGER, G. HILSCHER and R. GROESSINGER, *J. Less-Common Metals* **131** (1987) 409.
29. G. WIESINGER, G. HILSCHER, R. GROESSINGER, S. HEISZ and H. KIRCHMAYR, Proceedings 6th World Hydrogen Energy Conference (WHEC VI), 20 to 24 July,

1986, Vienna, Austria.
30. D. FRUCHART, P. WOLFERS, J. D. M. COEY, P. VULLIET, A. YAOUANC, P. L'HERITIER and R. FRUCHART, Proceeings International Symposium on the Properties and Application of Metal Hydrides V (ISPAMH V), 23 to 25 May, 1986, Maubuisson, France. Abstract in *J. Less Common Metals* **131** (1987) 212.
31. K. H. J. BUSCHOW, in Handbook on the Physics and Chemistry of Rare Earths, Vol. 6, edited by K. A. Gschneidner Jr and L. Eyring (1984) p. 1.
32. Micro-X program package, MS DOS version, B. Rupp (1986).
33. Lazy Pulverix Program, K. YVON, W. JEITSCHKO and E. PARTHE, *J. Appl. Crystallogr.* **10** (1977) 7; updated interactive VAX/VMS version B. Rupp, Vienna (1985).
34. J. W. HERBST, J. J. CROAT, R. W. LEE and W. B. YELON, *J. Appl. Phys.* **53** (1982) 250.
35. H. H. STADELMAIER, G. SCHNEIDER and M. ELLNER, *J. Less-Common Metals* **115** (1986) L11.
36. I. E. GLADYSHEVSKY, B. YA. KOTUR, O. I. BODAK and U. R. SVORCHUK, *Dokl. Akad. Nauk Ukr. SSR Ser. A* (1977) 751.
37. D. GIVORD, H. S. LI and J. M. MOREAU, *Solid State Commun.* **50** (1984) 497.
38. L. SCHLAPBACH, A. SEILER, F. STUCKI and H. C. SIEGMANN, *J. Less-Common Metals* **73** (1980) 145.
39. L. P. FERREIRA, R. GUILLEN, P. VULLIET, A. YAOUANC, D. FRUCHART, P. WOLFERS, P. L'HERITIER and R. FRUCHART, *J. Mag. Magn. Mater.* **53** (1985) 145.
40. P. DALMAS DE REOTIER, D. FRUCHART, L. PONTONNIER, F. VAILLANT, P. WOLFERS, A. YAOUANAC, J. M. D. COEY, R. FRUCHART and PH. L'HERITIER, *J. Less-Common Metals* **129** (1987) 133.
41. A. STERN, A. RESNIK and D. SHALTIEL, *ibid.* **88** (1982) 431.
42. A. RESNIK, M. RESHOTKO, B. RUPP and D. SHALTIEL, to be published.
43. J. A. DEAN, (ed.), "Lange's Handbook of Chemistry", 11sth Edn (McGraw-Hill, 1974).
44. B. RUPP and P. FISCHER, Prog. Rep. LNS-EIR, 1987, ETH Zurich, in press.
45. B. RUPP and G. WIESINGER, *J. Magn. Magn. Mater*, in press.
46. K. H. J. BUSCHOW, *J. Less-Common Metals* **11** (1966) 204.
47. A. E. RAY, *Acta Crystallogr.* **21** (1966) 426.
48. V. K. AGARVAL and R. N. KUZ'MIN, *Sov. Phys.-Crystallogr.* **16** (1972) 670.
49. A. BEZINGE, H. F. BRAUN, J. MULLER and K. YVON, *Solid State Commun.* **55** (1985) 131.
50. D. GIVORD, P. TENAUD and J. M. MOREAU, *J. Less-Common Metals* **115** (1986) L7.
51. *Idem, ibid.* **123** (1986) 109.
52. A. BEZINGE, K. YVON, H. F. BRAUN and J. MULLER, *Phys. Rev. B,* in press.
53. D. B. DEMOOIJ and K. H. J. BUSCHOW, *Philips J. Res.* **41** (1986) 400.
54. F. SPADA, C. ABACHE and H. OESTERREICHER, *J. Less-Common Metals* **99** (1984) L21.
55. H. OESTERREICHER, F. SPADA and C. ABACHE, *Mater. Res. Bull.* **19** (1984) 1069.
56. H. BOLLER and H. OESTERREICHER, *J. Less-Common Metals* **103** (1984) L5.
57. C. B. SHOEMAKER, D. P. SHOEMAKER and R. FRUCHART, *Acta Crystallogr.* **40** (1984) 1665.
58. C. ABACHE and H. OESTERREICHER, *J. Appl. Phys.* **60** (1986) 1114.
59. J. W. HERBST, J. J. CROAT and W. B. YELON, *ibid.* **57** (1985) 4086.
60. O. M. DUB, N. F. CHABAN and YU. B. KUZ'MA, *J. Less-Common Metals* **117** (1986) 297.
61. O. M. DUB and YU. B. KUZ'MA, *Poroshk. Metall.* **7** (1986) 49.
62. J. F. HERBST, J. J. CROAT, E. F. PINKERTON and W. B. YELON, *Phys. Rev. B* **29** (1984) 4176.
63. M. Q. HUANG, E. B. BOLTICH and W. E. WALLACE, *J. Less-Common Metals* **124** (1986) 55, (parameter a_0 mistyped as 8.709).
64. H. YAMAMOTO, Y. MATSUURA, S. FUJIMURA and M. SAGAWA, *Appl. Phys. Lett.* **45** (1984) 1141.
65. S. SINNEMA, R. J. RADWANSKI, J. J. M. FRANSE D. B. DEMOOIJ and K. H. J. BUSCHOW, *J. Mag. Magn. Mater.* **44** (1984) 333.
66. C. ABACHE and H. OESTERREICHER, *J. Appl. Phys.* **57** (1985) 4112.

Received 8 June
and accepted 20 August 1987